Chinese Chemical Letters 32 (2021) 1502–1506

Contents lists available at ScienceDirect

Chinese Chemical Letters

journal homepage: www.elsevier.com/locate/cclet

Communication

Hydrothermal synthesis of hierarchical SnO_2 nanomaterials for high-efficiency detection of pesticide residue

Haijie Cai[a,e,1], Xiaopeng Qiao[a,1], Meilian Chen[b], Dongsheng Feng[b], Abdulaziz A. Alghamdi[c], Fahad A. Alharthi[c], Yingjie Pan[a], Yong Zhao[a], Yongheng Zhu[a,*], Yonghui Deng[d,e]

[a] College of Food Science and Technology, Laboratory of Quality & Safety Risk Assessment for Aquatic Products on Storage and Preservation (Shanghai), Ministry of Agriculture and Shanghai Engineering Research Center of Aquatic-Product Processing & Preservation Shanghai Ocean University, Shanghai 201306, China
[b] Shanghai Agricultural Product Quality and Safety Center, Shanghai 201306, China
[c] Department of Chemistry, College of Science, King Saud University, P.O. Box 2455, Riyadh 11451, Saudi Arabia
[d] Department of Chemistry, Fudan University Shanghai 200433, China
[e] State Key Lab of Transducer Technology, Shanghai Institute of Microsystem and Information Technology, Chinese Academy of Sciences, Shanghai 200050, China

ARTICLE INFO

Article history:
Received 9 September 2020
Received in revised form 30 September 2020
Accepted 21 October 2020
Available online 22 October 2020

Keywords:
SnO_2 nanomaterials
Hollow nanostructures
Hydrothermal methods
Acephate gas sensor
High-efficiency detection

ABSTRACT

Acephate pesticide contamination in agricultural production has caused serious human health problems. Metal oxide semiconductor (MOS) gas sensor can be used as a portable and promising alternative tool for efficiently detection of acephate. In this study, hierarchical assembled SnO_2 nanosphere, SnO_2 hollow nanosphere and SnO_2 nanoflower were synthesized respectively as high efficiency sensing materials to build rapid and selective acephate pesticide residues sensors. The morphologies of different SnO_2 3D nanostructures were characterized by various material characterization technology. The sensitive performance test results of the 3D SnO_2 nanomaterials towards acephate show that hollow nanosphere SnO_2 based sensor displayed preferable sensitivity, selectivity, and rapid response (9 s) properties toward acephate at the optimal working temperature (300 °C). This SnO_2 hollow nanosphere based gas sensor represents a useful tool for simple and highly effective monitoring of acephate pesticide residues in food and environment. According to the characterization results, particularly Brunauer-Emmett-Teller (BET) and Ultraviolet-Visible Spectroscopy (UV–vis), the obvious and fast response can be attributed to the mesoporous hollow nanosphere structure and appropriate band gap of SnO_2 hollow nanosphere.

Acephate, as a substitute for methamidophos, has been one of the effective insecticides to control pests on grains, fruits and vegetables for its low toxicity and high efficiency [1,2]. However, acephate preparation used in agricultural production were found to be poorly stable and bioactivation metabolized to methamidophos with extremely high selective mammalian toxicity [3]. Accordingly, the production and use of acephate has been banned in some countries and regions for its potential toxicity. Therefore, the rapid and effective detection of acephate is of great significance to supervise and standardize the use of pesticides and ensure food safety. At present, a variety of analytical techniques have been applied to detect acephate insecticides, such as colorimetry, fluorescence analysis, High-performance Liquid Chromatography (HPLC) and enzyme inhibition [4–8]. These conventional acephate detection methods show excellent accuracy and low detection limit. However, these methods are only applicable in laboratory analysis owing to the precondition of relatively complicated pretreatments, time-consuming operation, expensive equipment and experienced staff. Herein, it is still indispensable to develop a portable and effective detecting equipment for the on-site determination of acephate.

Gas sensors based on metal oxide semiconductors (MOS) provide fast response, good stability, low cost and low power consumption detection methods [9]. Synthesis of nanomaterials with controllable morphology is currently a hot field of gas sensor research [10,11]. Among them, tin dioxide (SnO_2) nanomaterials with controllable morphology have attracted extensive research

* Corresponding author.
E-mail address: yh-zhu@shou.edu.cn (Y. Zhu).
[1] These authors contributed equally to this work.

https://doi.org/10.1016/j.cclet.2020.10.029
1001-8417/

on account of their favorable physical and chemical properties [12,13]. So far, SnO_2 materials of various shapes have been successfully synthesized, such as nanoparticles, nanorods, nanobelts, nanowires, nanosheets, hierarchical nanostructures and hollow sphere [14–24]. Among these, 3D SnO_2 nanomaterials such as hierarchical nanostructures and hollow sphere possess porous structures, which attracts more studies for sensor application [25,26]. Huang *et al.* [27] reported a simple method for rapid detection of pesticide residues based on SnO_2 semiconductor gas sensor, which used the rectangular temperature model to detect and distinguish acephate, trichlorfon and their mixtures. However, researches on SnO_2 based gas sensor for pesticide residue detection are very rare.

In this study, variant hierarchical assembled SnO_2 nanosphere, SnO_2 hollow nanosphere and SnO_2 nanoflower were synthesized successfully *via* simple hydrothermal technique and subsequent calcination [28], and made into gas sensors for sensitively and selectively detection of acephate pesticide residues. The SnO_2 hollow nanospheres were synthesized successfully after a classical Ostwald ripening process in the absence of any template [29]. Then, SnO_2 nanosphere and SnO_2 nanoflower were successfully synthesized by changing tin source, hydrothermal reaction conditions, and adding surfactant. By comparing the acephate gas sensing performance among the three SnO_2 3D nanostructures, it is found that the SnO_2 hollow nanosphere not only got the highest response value, but also exhibited excellent selectivity and stability, as while as faster response speeds than that of the other two materials (SnO_2 nanosphere and SnO_2 nanoflower) [30]. In addition, the sensing reaction process was also discussed in this study to help explain the effect of hollow nanosphere structure of high sensing performance.

The main evolving process of synthesizing SnO_2 nanomaterials are shown in Fig. 1. As Fig. 1 shown, the sphere-like SnO_2 nanomaterial was synthesized by taken $SnCl_4{\cdot}5H_2O$ as the precursor without any surfactant in the reaction system. In the specific synthesis process, the complex $Sn[(OH)_6]^{2-}$ first rapidly decomposed to form large number of SnO_2 nuclei, and then these nuclei spontaneously aggregate to form nanoparticles. As the continuation of the hydrothermal reaction, tiny SnO_2 crystals gradually grow to form a unique SnO_2 nanosphere [31]. SnO_2 hollow nanosphere was controlled synthesis by taking potassium Stannate as tin source based on the Ostwald-ripening reaction [29]. The SnO_2 nanoflower was prepared by choosing $SnCl_2{\cdot}2H_2O$ as reactant and $Na_3C_6H_5O_7$ as surfactant. In the presence of $Na_3C_6H_5O_7$, the rapid precipitation of $Sn(OH)_2$ was inhibited, resulting in anisotropic growth of SnO_2 crystals in [101] direction and the formation of SnO_2 single nanosheet. However, the surface energy of a single nanosheet is quite high and needs to be reduced by reducing the exposed area [32,33]. Herein, the SnO_2 nanoflower was synthesized successfully through the self-assemble of single nanosheet.

As shown in Fig. 2, SEM and TEM observations were taken to illustrate the microstructures of SnO_2 nanosphere, SnO_2 hollow nanosphere and SnO_2 nanoflower firstly. Figs. 2a–c show the SEM and TEM images of SnO_2 nanospheres. Obviously, SnO_2 nanospheres have a clear morphology and microstructure, with a size of about 250−400 nm. Figs. 2d–f show the morphological structure images of SnO_2 hollow nanosphere. The particle diameter SnO_2 hollow nanosphere is about 350−450 nm, and the shell thickness is about 30−50 nm. SnO_2 nanoflower structure consists of 20 nm thick nanosheets were also clearly observed in Figs. 2g–i. The HRTEM images of the as-synthesized three SnO_2 nanomaterials are also displayed in the inset images of Figs. 2c, f and i. The lattice spacings of SnO_2 nanosphere, SnO_2 hollow nanosphere and SnO_2 nanoflower nanomaterials were estimated to be 0.335 nm, 0.336 nm and 0.335 nm, respectively, and all corresponding to [101] reflections of rutile SnO_2 [34].

The crystal structures of the as synthesized SnO_2 nanosphere, SnO_2 hollow nanosphere and SnO_2 nanoflower nanomaterials were studied by XRD analysis. Typical diffraction patterns were illustrated in Fig. 3a. All diffraction peaks of the three materials correspond well to the JCPDS No. 41-1445 card, which confirm the tetragonal rutile phase of the synthesized SnO_2 nanosphere, SnO_2 hollow nanosphere and SnO_2 nanoflower. No extra characteristic peaks were found, showing that the excellent purity of the SnO_2 nanomaterials [35–37]. What worth motioning is that the [101] crystal surface diffraction peak of SnO_2 nanoflower is relative stronger than that of the standard card. This is mainly due to the adsorption of $Sn(OH)^{2-}$ growth on the surface [101], which may conducive to the anisotropic growth of SnO_2 crystals along the direction [101].

XPS was employed to analyze the chemical states of the SnO_2 nanosphere, SnO_2 hollow nanosphere, and SnO_2 nanoflower. The

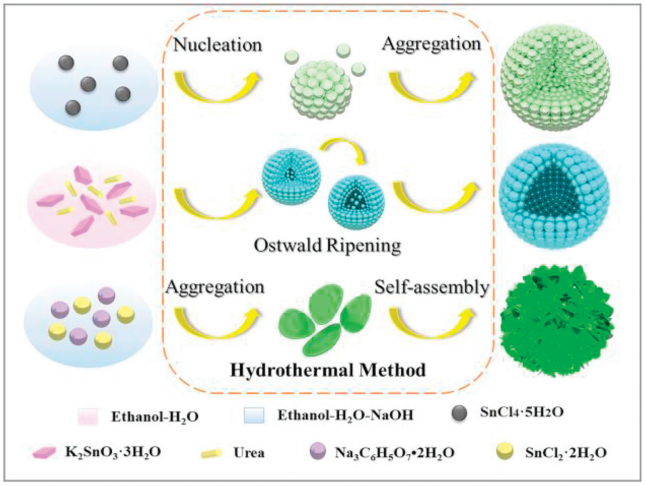

Fig. 1. Schematic diagram of the control synthesis of SnO_2 nanosphere, SnO_2 hollow nanosphere and SnO_2 nanoflower *via* a simple template-free process.

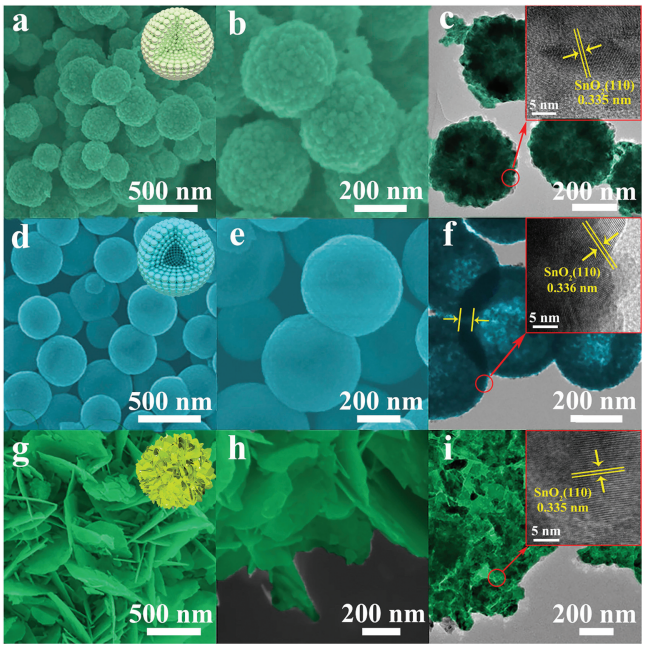

Fig. 2. SEM, TEM and HRTEM of SnO_2 nanomaterials in different morphologies: (a-c) SnO_2 nanosphere, (d-f) SnO_2 hollow nanosphere and (g-i) SnO_2 nanoflower.

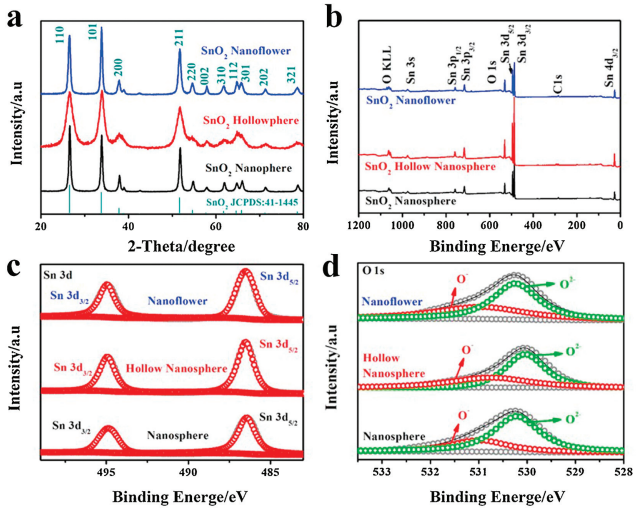

Fig. 3. (a) XRD patterns of as-synthesized SnO_2 nanosphere, SnO_2 hollow nanosphere and SnO_2 nanoflower. (b) Survey, (c) Sn 3d, (d) O 1s high resolution XPS spectrum of as-synthesized SnO_2 nanomaterials.

complete spectra are shown in Fig. 3b. The peaks completely in accordance to Sn and O are exactly the only peaks observed in the as-prepared SnO_2 nanosphere, hollow nanosphere and nanoflower materials, indicating the excellent monodispersity of the three samples. Sn 3d in high-resolution XPS spectra (Fig. 3c) shows that the typical characteristics of Sn^{4+} in tetragonal SnO_2. It is clearly shown in Fig. 3d that the lower binding energy of corresponds to the absorbed oxygens (O^-: 531.2 eV) of SnO_2, whereas the other binding energy corresponds to the lattice oxygen (O^{2-}: 530.3 eV) chemical states of oxygen in the three SnO_2 nanomaterials, respectively [38,39]. Obviously, there are no significant differences in the valence states of tin and oxygen in the materials with different morphologies.

The results of nitrogen adsorption-desorption isotherms test (Fig. S1 in Supporting information) and Barrett-Joyner-Halenda (BJH) analysis (Table S1 in Supporting information) clearly show the surface adsorption property of the above sensing nanomaterial. The Brunauer-Emmett-Teller (BET) tests of the SnO_2 nanosphere, SnO_2 hollow nanosphere, and SnO_2 nanoflower all have a hysteresis loop (Fig. S1), which is consistent with typical type-IV [40], showing the mesoporous structure of as-synthesized 3D nanomaterials [41]. SnO_2 with hollow nanosphere structure possess the largest surface area (28.3 m^2/g STP), while, SnO_2 nanosphere (14.8 m^2/g STP) and SnO_2 nanoflower (19.6 m^2/g STP) show lower surface area, respectively.

Based on the synthesized SnO_2 nanomaterials with different morphologies, we further prepared SnO_2 nanosphere, SnO_2 hollow nanosphere, and SnO_2 nanoflower based gas sensors, for the systematic analysis of the gas sensitivity of SnO_2 nanostructures in the rapid detection of acephate. The operating temperature tests (200–400 °C) of sensors based on SnO_2 nanosphere, SnO_2 hollow nanosphere, and SnO_2 nanoflower were proceed in 20 ppm acephate. As Fig. 4a shown, all gas sensors display the crest value at an operating temperature of 300 °C. The acephate response value increases before the working temperature reach up to 300 °C, and dramatic decreases as operating temperature continue to rise. Furthermore, it can be clearly seen from Fig. 3a that the SnO_2 hollow nanosphere has the highest sensitivity (R_{air}/R_{gas} = 11.87), followed by the SnO_2 nanoflower (R_{air}/R_{gas} = 9.23), and the SnO_2 nanosphere (R_{air}/R_{gas} = 3.95) shows the lowest gas sensing response. This mainly on account of hollow structure has larger specific surface area than solid spherical structure, which is more conducive to the redox reaction of the gas, so that it has a higher

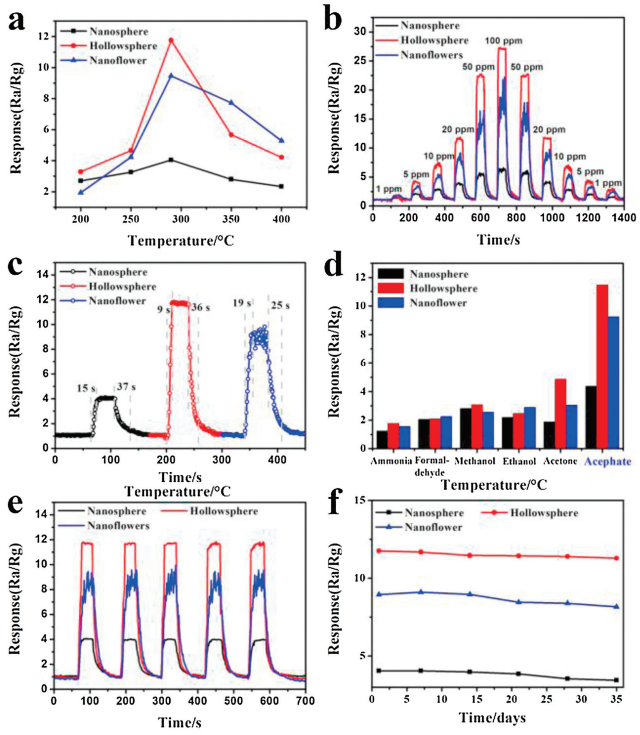

Fig. 4. Typical sensing responses of the SnO_2 nanosphere, SnO_2 hollow nanosphere and SnO_2 nanoflower based sensors: (a) The temperature-dependent sensitivity of various sensors *versus* the operating temperature from 200 °C to 400 °C towards 20 ppm acephate. (b) Dynamic acephate (1-100 ppm) sensing transients. (c) Response/recovery times of the preparative sensors. (d) Selectivity of gas sensor towards acephate at 300 °C. (e) Five periods of response curve and f representative long-term stability curve of SnO_2 based sensor to 20 ppm acephate at 300 °C.

sensitivity [42]. Gas sensor based on nanoflower structure shows better sensitivity than that of nanospheres mainly due to its interlaced thin nanostructures on the surface of nanoflower increase the reaction between acephate molecules and materials to a certain extent. However, as shown in Figs. 4b, c and e, it is possible that the interlaced thin nanostructures on the surface of the nanoflower caused its unstable gas response.

Dynamic response of SnO_2 nanosphere, SnO_2 hollow nanosphere, and SnO_2 nanoflower towards different concentrations of acephate (1–100 ppm) were then investigated at 300 °C. As Fig. 4b clearly illustrates, the response value of the obtained SnO_2 nanosphere, SnO_2 hollow nanosphere, and nanoflower based sensors all increased with the injection quantity of acephate increasing from 1 ppm to 100 ppm, and decreased with the concentration decreasing, which indicates that the gas sensors have distinguished reversibility and repeatability. What worth mentioning is that the SnO_2 hollow nanosphere based gas sensor also shows good linearity with the acephate concentration. Fig. 4c displays the response/recovery behavior of sensors toward 20 ppm acephate. SnO_2 hollow nanosphere shows relative fast response speed (9 s) upon exposure to acephate in those of SnO_2 nanosphere (15 s) and nanoflower (19 s). According to the results of BET tests, SnO_2 nanospheres hollow structures with more surface area, which exposes larger effective response area for sensor testing than the other materials. Meanwhile, the mesoporous structures in the materials also contribute to the smooth diffusion of target molecules in SnO_2 hollow nanospheres [43]. Therefore, SnO_2 hollow nanospheres show the highest response and shortest response-recovery time to the target gases under the same conditions of the three nanomaterials.

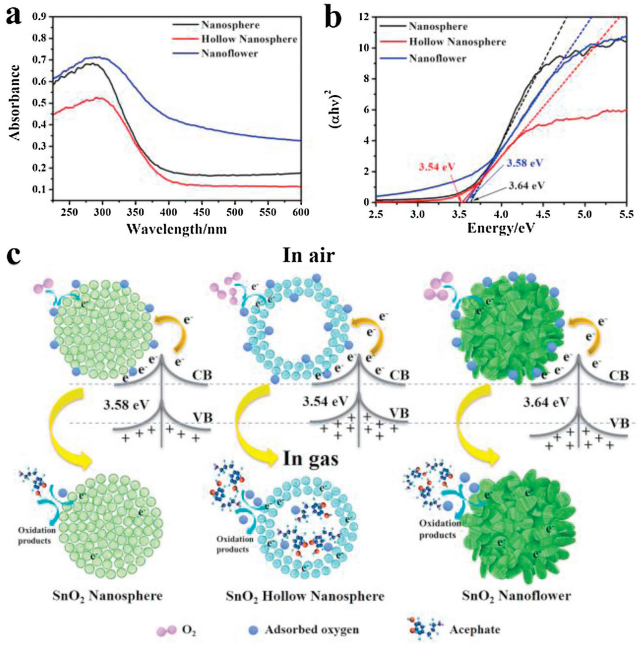

Fig. 5. (a) UV–vis diffuse reflectance spectrum. (b) Kubelka-Munk function curve plotted against photon *versus* the energy of absorbed light of SnO_2 nanosphere, SnO_2 hollow nanosphere and SnO_2 nanoflower. (c) The reaction schematic diagram of the gas sensor based on 3D SnO_2 nanomaterials in air and acephate.

Selectivity is the most important criterion for gas sensors in real-time application. Hence, this work also investigated the sensitivities of SnO_2 nanosphere, SnO_2 hollow nanosphere and SnO_2 nanoflower based sensors, when explore to the common various interfering gases, including acetone, ethanol, methanol, formaldehyde and ammonia under the same conditions (Fig. 4d). Obviously, the above characteristic curves indicate that SnO_2 hollow nanosphere based sensor has a good selectivity to acephate of 20 ppm and less affected by other gases at 300 °C, which is beneficial to the effective differentiation of acetylate.

In addition, repeatability and long-term stability tests were conducted on the on-site test of acephate (Figs. 4e and f). The good repeatability was confirmed by exposure to 20 ppm of acephate for five times under the same conditions. During the continuously five-week of testing, the sensitivity of all sensors displays minor changes towards 20 ppm acephate at 300 °C, showing an excellent sensor stability of the SnO_2 nanomaterials-based sensor. Results of above tests indicate the good repeatability and stability of the as-fabricated acephate sensor. These excellent gas sensitivity characteristics are conducive to the application and promotion of the as-prepared gas sensors.

The main reason for good sensing properties of SnO_2 hollow nanosphere is the stable crystal and mesoporous hollow structure. The band gap of SnO_2 nanomaterials with different morphologies can be obtained by UV–vis diffuse reflectance spectra in the Fig. 5a [44]. The band gap of SnO_2 nanosphere and SnO_2 nanoflower are 3.64 eV and 3.58 eV, respectively. As actually shown in Fig. 5b, SnO_2 hollow nanosphere has the minimum bandgap energy of 3.54 eV, which means that it is more liable for the electrons of SnO_2 hollow nanosphere to transition from its valence to the conduction band [45–47]. Great quantity of carrier can be more easily transferred to the conductive band of SnO_2 hollow nanosphere, resulting in the more significant change in the conductivity of the material (Fig. 5c). Furthermore, as shown in Fig. 5c, hollow nanospheres with huge specific surface area provide active sites on and inside the surface, which can be used for oxygen adsorption, and acted as sensitizers to modify and display their functions [48]. Therefore, the response of hollow nanosphere is higher than the SnO_2 nanosphere and SnO_2 nanoflower. Therefore, the SnO_2 hollow nanospheres sensor shows the best sensing performance for acephate in different SnO_2 hollow nanomaterials.

In summary, SnO_2 nanosphere, SnO_2 hollow nanosphere and SnO_2 nanoflower with characteristic structure were prepared through one-step template free method, by controlling the acid base of reaction and changing reaction temperature. Furthermore, the effect of morphology on gas-sensing behavior were studied. Experimental results show that MOS gas sensors based on SnO_2 with different morphologies have the superiority of good sensitivity, high stability, and rapid response recovery to acephate at 300 °C. SnO_2 hollow structure shows the highest sensitivity, by comparation of the gas sensing behavior with the SnO_2 nanosphere and SnO_2 nanoflower based sensors. This is mainly due to the large surface area of the hollow structure, which can expose the rich reaction points for target molecules, thereby helping to improve the sensitivity. This SnO_2 hollow nanosphere based gas sensor provides a vital research direction for the development of a new, simple, accurate and rapid sensor for monitoring acephate pesticide residue.

Declaration of competing interest

The authors report no declarations of interest.

Acknowledgments

This work was financially funded by the National Natural Science Foundation of China (No. 31701678), the Key Project of Shanghai Agriculture Prosperity through Science and Technology (No. 2019-02-08-00-15-F01147), the project of Shanghai Science and Technology Committee (No. 19391901600), the Key Basic Research Program of Science and Technology Commission of Shanghai Municipality (No. 20JC1415300), the State Key Laboratory of Transducer Technology of China (No. SKT1904), and the Research Support Project number (No. RSP-2020/155), King Saud University, Riyadh, Saudi Arabia.

Appendix A. Supplementary data

Supplementary material related to this article can be found, in the online version, at doi:https://doi.org/10.1016/j.cclet.2020.10.029.

References

[1] M. Mahajna, G.B. Quistad, J.E. Casida, Chem. Res. Toxicol. 10 (1997) 64–69.
[2] H. Sharma, R. Mutharasan, Sensor. Actuat. B: Chem. 183 (2013) 535–549.
[3] S. Mostafalou, M. Abdollahi, Arch. Toxicol. 91 (2017) 549–599.
[4] P. Kumar, K.H. Kim, A. Deep, Biosens. Bioelectron. 70 (2015) 469–481.
[5] M. Pabbi, S.K. Mittal, Anal. Methods 9 (2017) 1672–1680.
[6] C.S. Pundir, A. Malik, Biosens. Bioelectron. 140 (2019) 111348.
[7] Y. Shen, F. Yan, X. Huang, et al., RSC Adv. 6 (2016) 88096–88103.
[8] P. Raghu, T.R. Madhusudana, K. Reddaiah, et al., Food Chem. 142 (2014) 188–196.
[9] N. Luo, B. Zhang, D. Zhang, J. Xu, Chin. Chem. Lett. 31 (2020) 2033–2036.
[10] L. Deng, L. Bao, J. Xu, et al., Chin. Chem. Lett. 31 (2020) 2041–2044.
[11] Z. Chen, D. Wang, X. Wang, et al., Chin. Chem. Lett. 31 (2020) 2063–2066.
[12] Q. Zhou, L. Yang, G. Wang, et al., Biosens. Bioelectron. 49 (2013) 25–31.
[13] Y. Xu, L. Zheng, C. Yang, et al., ACS Appl. Mater. Interfaces 12 (2020) 20704–20713.
[14] M.A.H. Khan, M.V. Rao, Q. Li, Sensors 19 (2019) 905.
[15] X. Liu, N. Chen, B. Han, et al., Nanoscale 7 (2015) 14872–14880.
[16] J. Shin, S.J. Choi, I. Lee, et al., Adv. Funct. Mater. 23 (2013) 2357–2367.
[17] X. Kou, N. Xie, F. Chen, et al., Sensor. Actuat. B: Chem. 256 (2018) 861–869.
[18] M.M. Arafat, B. Dinan, S.A. Akbar, A.S. Haseeb, Sensors 12 (2012) 7207–7258.
[19] M. Shojaee, S. Nasresfahani, M.H. Sheikhi, Sensor. Actuat. B: Chem. 254 (2018) 457–467.
[20] G. Singh, R.C.Singh Virpal, Sensor. Actuat. B: Chem. 282 (2019) 373–383.
[21] L. Wang, Y. Wang, K. Yu, et al., Sensor. Actuat. B: Chem. 232 (2016) 91–101.
[22] J.S. Chen, X.W. Lou, Small 9 (2013) 1877–1893.
[23] Y. Li, S. Wang, P. Hao, et al., Sensor. Actuat. B: Chem. 273 (2018) 751–759.

[24] G.D. Park, J.H. Kim, Y.C. Kang, Nanoscale 10 (2018) 13531–13538.
[25] H. Yang, X. Bai, P. Hao, et al., Sensor. Actuat. B: Chem. 280 (2019) 34–40.
[26] X. Wang, F. Liu, X. Chen, et al., Powder Technol. 364 (2020) 159–166.
[27] X. Huang, L. Wang, Y. Sun, F. Meng, J. Liu, Sensor. Actuat. B: Chem. 99 (2004) 330–335.
[28] X. Dou, D. Sabba, N. Mathews, et al., Chem. Mater. 23 (2011) 3938–3945.
[29] X.W. Lou, Y. Wang, C. Yuan, J.Y. Lee, L.A. Archer, Adv. Mater. 18 (2006) 2325–2329.
[30] J.L. Tian, J. Wang, Y.W. Hao, et al., Sensor. Actuat. B: Chem. 202 (2014) 795–802.
[31] W. Zeng, H. Zhang, Y. Li, et al., Mater. Res. Bull. 57 (2014) 91–96.
[32] W. Zeng, Q. He, K. Pan, Y. Wang, Phys. E 54 (2013) 313–318.
[33] D. Zhang, J. Liu, C. Jiang, A. Liu, B. Xia, Sensor. Actuat. B: Chem. 240 (2017) 55–65.
[34] W. Xin, T. Gao, W. Zhang, et al., J. Alloys Compd. 784 (2019) 157–164.
[35] D. Xue, P. Wang, Z. Zhang, Y. Wang, Sensor. Actuat. B: Chem. 296 (2019)126710.
[36] R. Peng, J. Chen, X. Nie, et al., J. Alloys Compd. 762 (2018) 8–15.
[37] P. Manjula, R. Boppella, S.V. Manorama, ACS Appl. Mater. Interfaces 4 (2012) 6252–6260.
[38] R.G. Motsoeneng, I. Kortidis, S.S. Ray, D.E. Motaung, ACS Omega 4 (2019) 13696–13709.
[39] G. Singh, R.C. Singh, J. Electron. Mater. 48 (2019) 4478–4490.
[40] X. Xiao, L. Liu, J. Ma, et al., ACS Appl. Mater. Interfaces 10 (2018) 1871–1880.
[41] L. Yang, Z. Wang, X. Zhou, et al., RSC Adv. 8 (2018) 24268–24275.
[42] D. Wang, L. Deng, H. Cai, et al., ACS Appl. Mater. Interfaces 12 (2020) 18904–18912.
[43] Y.J. Jeong, W.T. Koo, J.S. Jang, Nanoscale 10 (2018) 13713–13721.
[44] A. Kar, S. Kundu, A. Patra, J. Phys. Chem. C 115 (2011) 118–124.
[45] D. Wang, S. Huang, H. Li, et al., Sensor. Actuat. B: Chem. 282 (2019) 961–971.
[46] Y. Zhu, D. Wang, L. Zhang, et al., RSC Adv. 3 (2013) 10154–10157.
[47] Y. Zhang, X. Liu, P. Li, Nano Energy 56 (2019) 733–740.
[48] Y. Zhu, Y. Zhao, J. Ma, et al., J. Am. Chem. Soc. 139 (2017) 10365–10373.